ACS APPLIED MATERIALS & INTERFACES

Research Article

www.acsami.org

Acceleration of Proteolytic Activity Associated with Selection of Thiol Ligand Coatings on Quantum Dots

Miao Wu and W. Russ Algar*

Department of Chemistry, University of British Columbia, 2036 Main Mall, Vancouver, British Columbia V6T 1Z1, Canada

Supporting Information

ABSTRACT: Nanoparticle bioconjugates are attractive probes for measuring the activity of hydrolytic enzymes. In these configurations, the localization of multiple copies of a hydrolase substrate to a nanoparticle scaffold has been reported to enhance apparent activity by factors of 2 to 3 compared to that for equivalent amounts of substrate in bulk solution. Here, we studied the effect of surface chemistry on protease activity using multivalent QD–peptide substrate conjugates as a model system. QDs were coated with cysteine (CYS), glutathione (GSH), dihydrolipoic acid (DHLA), or 3-mercaptopropionic acid (MPA) ligands, and thrombin and trypsin were used as model proteases. Proteolytic activity was measured for different combinations of ligand and protease using Förster resonance energy transfer (FRET)-based assays. The highest levels of activity were observed with CYS and GSH coatings, and the lowest levels of activity were observed with DHLA and MPA coatings. In all cases, proteolytic activity was accelerated compared to that for an equivalent amount of substrate in bulk solution, with up to 80- and 65-fold increases in the apparent specificity constants for thrombin and trypsin, respectively. Thrombin was more strongly affected by the QD surface chemistry, with up to a 50-fold variation in its apparent specificity constant between ligand coatings, whereas only a 5-fold variation was observed with trypsin. These trends were correlated to adsorption of the proteases on the QDs and are discussed in the context of the physicochemical properties of both components. This work clearly indicates a critical role for the nanoparticle interface in mediating substrate turnover and provides some of the strongest support to date for a so-called hopping model of activity.

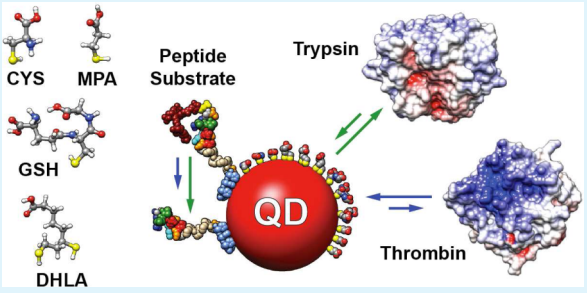

KEYWORDS: *quantum dot, ligand, peptide, Förster resonance energy transfer, protease, hydrolytic activity*

INTRODUCTION

An immense variety of probes based on semiconductor quantum dots (QDs) and other nanoparticle materials have been developed for biosensing and other biological applications.[1−3] Several of these bioprobes have been designed to detect the activity of enzymes. Considering hydrolase enzymes in particular, a common format is to conjugate a central optically active nanoparticle such as a QD,[4] gold nanoparticle (AuNP),[5] or graphene oxide sheet[6] with a biomolecular substrate for the target enzyme. This substrate is often labeled with a dye or another nanoparticle at the opposite terminus such that energy transfer can occur between the central nanoparticle and the label.[7] Hydrolytic activity then cleaves the substrate such that the central nanoparticle and the label diffuse apart, resulting in a loss of energy transfer that can be tracked optically. In the case of QDs, Medintz et al.,[8] Shi et al.,[9] and Chang et al.[10] reported the first QD-based probes for detecting the activity of proteases, and Gill et al. reported QD-based probes for detecting nuclease activity.[11] Many other iterations and variations of these designs have been reported subsequently (for example, refs 12−15 and many others).

Whereas a multitude of biophysical studies on the activity of nanoparticle−enzyme conjugates toward substrates in bulk solution have been published (for a recent review, see ref 16), biophysical studies of the converse configuration, with substrate bound to the nanoparticle, have been relatively scarce. To date, the interest in such probes has almost exclusively been their analytical utility; however, a pair of recent studies on the kinetics of hydrolase activity toward nanoparticle−substrate conjugates has provided some interesting new insight. Prigodich et al. found that the activity of ribonuclease H (RNase H) toward multivalent AuNP−DNA/RNA heteroduplex conjugates was enhanced ∼2-fold relative to the same substrate in bulk solution.[17] The association of the RNaseH with the high density of DNA oligonucleotides around the AuNP resulted in colocalization of the enzyme with its RNA substrate, leading to enhanced activity. Similarly, Algar et al. reported that the net proteolytic activity associated with multivalent QD–peptide substrate conjugates was enhanced 3-fold and that the kinetics did not follow the classic Michaelis–Menten model.[18] The data was consistent with a hopping model where the localization of multiple peptide substrates to the QD, combined with weak interactions between the protease and poly(ethylene glycol) coating on

Received: October 27, 2014
Accepted: January 8, 2015
Published: January 21, 2015

ACS Publications © 2015 American Chemical Society

DOI: 10.1021/am507466b
ACS Appl. Mater. Interfaces 2015, 7, 2535−2545

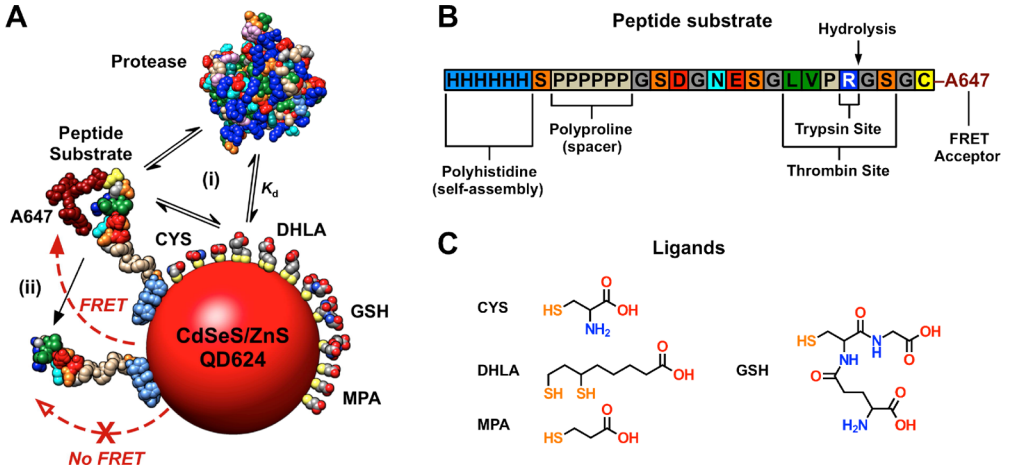

Figure 1. (A) Schematic of the QD-based proteolytic systems studied. CdSeS/ZnS QDs (peak PL at 624 nm) were coated with cysteine (CYS), dihydrolipoic acid (DHLA), glutathione (GSH), or 3-mercaptopropionic acid ligands (MPA) and self-assembled with a fluorescent dye (A647)-labeled peptide substrate, Sub(A647). The dye served as an acceptor for FRET with the QD donor. (i) Interactions between thrombin or trypsin and the QD–peptide conjugate led to (ii) protease-catalyzed hydrolysis of the peptide with loss of FRET. (B) Amino acid sequence of the peptide substrate. (C) Structures of the different small molecule thiol ligands used to coat the QDs.

the QDs, was responsible for the observed enhancement and kinetic profile.[18] However, the weak interactions between the protease and QD interface were not directly observable.[18] While both of the above examples suggest an important role for the nanoparticle as a scaffold for colocalizing enzyme and substrate, the enhancements in hydrolytic activity generated by this effect have thus far appeared to be relatively modest.

Here, we analyze the kinetics of proteolysis associated with multivalent QD–peptide substrate conjugates that have been prepared with four small molecule thiol ligand coatings. It is shown that the selection of ligand coating can lead to both dramatic and modest enhancements of proteolytic activity, and we link these observations to interactions between the enzyme and the QD interface. Two well-known serine proteases, trypsin and thrombin, are used in this study, with a Förster resonance energy transfer (FRET)-based configuration for tracking proteolysis. As illustrated in Figure 1, CdSeS/ZnS QDs with red emission (QD624) were coated with either cysteine (CYS), dihydrolipoic acid (DHLA), glutathione (GSH), or 3-mercaptopropionic acid (MPA) and then self-assembled with multiple copies of a peptide substrate. The peptide, which contained cleavage sites for both trypsin and thrombin, was labeled with a terminal Alexa Fluor 647 dye that functioned as FRET acceptor for the QD donor. Changes in FRET were used to quantitatively track proteolysis using a method described previously.[18] Depending on the choice of ligand coating on the QD and its adsorptive interactions with the protease, activity enhancements of up to 80-fold relative to substrate in bulk solution are possible, far exceeding those reported previously. Moreover, the comparison between trypsin and thrombin reveals that the effects of the coating also depend strongly on the physical properties of the protease. Overall, this work provides new biophysical insights into the mechanism underlying proteolytic activity associated with QD–peptide substrate conjugates, and nanoparticle–enzyme substrate conjugates more generally, providing much stronger support for the so-called hopping model than previous studies. Given the importance of proteases and other enzymes in numerous biological processes and as drug targets,[19−23] such insights are invaluable for the design of nanoparticle-based bioanalytical probes that exhibit improved sensitivity and selectivity toward their target enzymes.

EXPERIMENTAL SECTION

A summary of the main experimental methods is given below. Further details can be found in the Supporting Information.

Materials. CdSeS/ZnS core/shell QDs (CytoDiagnostics, Burlington, ON, Canada) with red emission (~6 nm, peak PL at 624 nm; QD624) or green emission (~6 nm, peak PL at 524 nm; QD524) were made water-soluble by coating with one of four different small molecule thiol ligands: glutathione (GSH), cysteine (CYS), dihydrolipoic acid (DHLA), or 3-mercaptopropionic acid (MPA). The ligand exchange procedures are described in detail in the Supporting Information. QDs were quantified by UV–visible spectrophotometry. A synthetic peptide (Bio-Synthesis Inc., Lewisville, TX) with a polyhistidine tag was labeled at a terminal cysteine residue with Alexa Fluor 647 (A647)-maleimide (Life Technologies, Carlsbad, CA) as described previously.[24] The peptide sequence was H_6SP_6GSD-GNESGLVPRGSGC (written N-terminal to C-terminal) and is abbreviated as Sub(A647). Bovine thrombin (THR), bovine trypsin (TRP), and N_α-tosyl-L-lysine chloromethyl ketone hydrochloride (TLCK) were obtained from Sigma-Aldrich (Oakville, ON, Canada). Borate buffered saline (BBS; pH 8.5, 50 mM, 13.7 mM NaCl, 0.27 mM KCl) was prepared in-house and sterilized by autoclaving.

Calibration Curves. Calibration samples were prepared by mixing X–QD624 (X = GSH, CYS, DHLA, or MPA, in reference to the ligand coating on the QD) with varying amounts of Sub(A647) and predigested Sub(A647) using two different methods. These methods are explained conceptually in the Results section. Full experimental details can be found in the Supporting Information. In both methods, the PL spectra of the calibration samples were measured and used to calculate A647/QD624 PL ratios. Predigested peptide was prepared by incubating Sub(A647) with thrombin or trypsin (25 μM) overnight, at room temperature, followed by irreversible inhibition of the proteases with three separate 5 μL additions of 25 mM TLCK (in DMSO) at 60 min intervals.

Enzyme Assays. Stock solutions of 0.4 μM X–QD624–$[Sub(A647)]_{16}$ conjugates (the subscript number denotes the average number of peptides per QD) were prepared by first diluting 320n pmol of Sub(A647) (20 μM, 16n μL) with BBS (35n μL) and then adding 20n pmol of X-QD624 (5.0 μM, 4n μL), where n was the number of samples to be assayed. The stock solutions were let stand for 30 min prior to assays. A series of solutions of either thrombin (0.04–20 μM, scaling by factors of two) or trypsin (0.5–240 nM, scaling by factors of two) were prepared in BBS. Aliquots (50 μL) of

DOI: 10.1021/am507466b
ACS Appl. Mater. Interfaces 2015, 7, 2535–2545

X−QD624−[Sub(A647)]$_{16}$ conjugate solution were added to an equal volume of the series of protease solutions in a 96-well microtiter plate (100 μL final volume, 0.20 μM final concentration of QD624). Immediately after mixing, the PL emission from the QD624 (measured at 624 nm) and the A647 (measured at 668 nm) were recorded at 2 min intervals over 4 h using 400 nm excitation. Details of assays without QDs are described in the Supporting Information.

QD-Inhibition Experiments. Inhibition experiments used X−QD524 as an inhibitor and used GSH−QD624−[Sub(A647)]$_{16}$ conjugates as a probe for protease activity. Aliquots from three separate stock solutions in BBS were combined prior to starting PL measurements: 33.3 μL of thrombin solution (5 μM), 33.3 μL X−QD524 (6.0 nM−3.0 μM, where X = GSH, CYS, DHLA, or MPA), and 33.3 μL GSH−QD624−[Sub(A647)]$_{16}$ conjugates (0.60 μM). The thrombin and X−QD524 were mixed first in the 96-well microtiter plate, followed by the addtion of the GSH−QD624−[Sub(A647)]$_{16}$ conjugates. PL emission from the GSH−QD624 and A647 was measured at 1 min intervals for 4 h. The final concentrations of thrombin and GSH−QD624−[Sub(A647)]$_{16}$ conjugate were 1.7 and 0.20 μM, respectively. Experiments with trypsin were done similarly except that the concentration of the added trypsin solution was 72 nM (final concentration of 24 nM). In both cases, two control samples without protease were run with (i) GSH−QD624−[Sub(A647)]$_{16}$ conjugates, to correct for any nonproteolytic changes in PL over time, and (ii) a combination of GSH−QD624−[Sub(A647)]$_{16}$ and X−QD524, to ensure that the peptide substrates did not dissociate from the original QD624 and reassemble on the QD524, generating a false positive signal for proteolysis.

Proteolytic Rate Analysis. For each time point, t, in an enzyme assay or inhibition assay, the A647/QD624 PL intensity ratio, ρ, was calculated using eq 1, where I_{QD624} and I_{A647} are the PL intensities of the QD624 and A647, respectively, and I_{668} and I_{624} are the measured PL intensities at 668 and 624 nm, respectively. The PL intensity measured at 624 nm was exclusively from the QD624; the PL intensity measured at 668 nm was predominantly from the A647 but did have a small contribution from the QD624. A correction factor, σ_{668} (= 0.04−0.05; see Supporting Information, Table S1), was used to account for the contribution from QD624.

$$\rho = \frac{I_{A647}}{I_{QD624}} = \frac{I_{668} - \sigma_{668} I_{624}}{I_{624}} \quad (1)$$

The PL ratios measured at time, t, and enzyme concentration, c, during an assay are denoted $\rho(t,c)$. For analysis, these PL ratios were normalized to control samples (no protease) according to eq 2, where $\bar{\rho}(t,c)$ is the normalized PL ratio.

$$\bar{\rho}(t,c) = \frac{\rho(t,c)}{\rho(t,0)}\rho(0,0) \quad (2)$$

The values of $\bar{\rho}(t,c)$ were converted to either the average number of Sub(A647) per QD, $N(t,c)$, or $\chi(t,c)$, the mole fraction of X−QD624−[Sub(A647)]$_{16}$ remaining, by comparison to calibration curves (*vide infra*). Progress curves were fit with eq 3 using nonlinear regression, where t_0 adjusts the starting position of the curve to account for the delay between adding enzyme and starting PL measurements, k_1 and k_2 are empirical rates, A_1 and A_2 are empirical amplitudes, and N_∞ is the residual peptide substrate per QD at long digestion times. The regressions were constrained so that (i) $A_1 + A_2 + N_\infty = N(0,0)$ and (ii) all progress curves in a data set shared the same value of t_0 (~2 min in most assays). Initial rates, v_0, were extracted from progress curves by taking the derivative of eq 3 at time $t = t_0$.

$$N(t,c) \text{ or } \chi(t,c) = A_1\, e^{-k_1(t-t_0)} + A_2\, e^{-k_2(t-t_0)} + N_\infty \quad (3)$$

RESULTS

Assay Format and FRET. To assay proteolytic activity, X−QD624−[Sub(A647)]$_{16}$ conjugates were mixed with either thrombin or trypsin, and the progress of the hydrolysis reaction was tracked in real time via changes in FRET. The X notation denotes a GSH, CYS, DHLA, or MPA ligand coating on the QD. The peptide substrate, Sub(A647), contained a LVPRGS amino acid sequence, which is a well-known cleavage site for thrombin[25] and, simultaneously, a cleavage site for trypsin. Hydrolysis occurred C-terminal to the arginine residue in both cases (see Figure 1B). A647 had its peak absorption at 647 nm (ε = 240 000 M^{-1} cm^{-1};[26] see Supporting Information, Figure S1) and was thus a good FRET acceptor for the QD624 donor. The spectral overlap integral between the QD and A647 was 1.96 × 10^{-9} mol^{-1} cm^6, corresponding to Förster distances of 3.3−6.7 nm for QD donor quantum yields between 0.001 and 0.06 for the various X−QDs (see Supporting Information, Table S2). With 400 nm excitation light, directly excited fluorescence from A647 was negligible, permitting tracking of proteolysis through changes in the ratio of FRET-sensitized A647 emission (peak at 668 nm) and FRET-quenched QD624 PL (i.e., A647/QD624 PL ratio). These two emission signals were easily resolved.

Calibration. Sub(A647) was hydrolyzed during proteolytic assays to yield unlabeled peptide fragments that remained bound to the QD and A647-labeled peptide fragments that either diffused away from the QD or nonspecifically adsorbed to the QD. Such adsorption can yield nontrivial background FRET. If FRET ratio data is to be converted into progress curves in terms of the number of Sub(A647), then it is necessary to account for any adsorption in calibration experiments. As in a previous study,[18] adsorption was taken into consideration by first predigesting substrate peptide, then mixing together both the predigested and native substrates at N:(N_0−N) ratios to generate calibration samples, where N_0 is the initial number of substrate peptides per QD in a proteolytic assays and $0 \le N \le N_0$. This method produces a mixture of native and digested peptide fragments on each QD. The assumption inherent to this procedure is that, during assays, individual substrate peptides are hydrolyzed in separate encounters between the QD−substrate conjugates and protease. Figure 2A(i) illustrates the conjugates expected from this model of proteolysis at the beginning, midpoint, and end of an assay. Figure 2B(i) shows an example of a calibration curve for GSH−QD624 with Sub(A647) and N_0 = 16. Analogous calibration curves for X−QD624 with X = CYS, DHLA, and MPA are shown in the Supporting Information (Figure S2).

The study that pioneered the above method of calibration ultimately suggested a so-called hopping model of proteolysis, where a protease hydrolyzes all of the substrate peptide conjugated to a QD in a single encounter.[18] At the midpoint of an assay, it would therefore be expected that half of the QD−substrate conjugates are completely undigested and half are fully digested, as illustrated in Figure 2A(ii). However, neither the above study nor other studies have proposed a calibration method that parallels a hopping model. To this end, we mixed undigested QD−substrate conjugates with fully digested conjugates at ratios of χ:(1 − χ), where χ is the mole fraction of undigested conjugates. Figure 2B(ii) shows an example of a calibration curve for GSH−QD624 with Sub(A647) prepared in this manner. It is notable that the calibration data are nearly identical. This agreement is expected theoretically when FRET ratios scale linearly with the number of acceptors per donor, as was the case for Sub(A647) with X−QD624 (see Supporting Information for details). More importantly, this result indicates that the two different models of proteolysis will yield the same apparent progress curves when measured via QD-FRET. For

DOI: 10.1021/am507466b
ACS Appl. Mater. Interfaces 2015, 7, 2535−2545

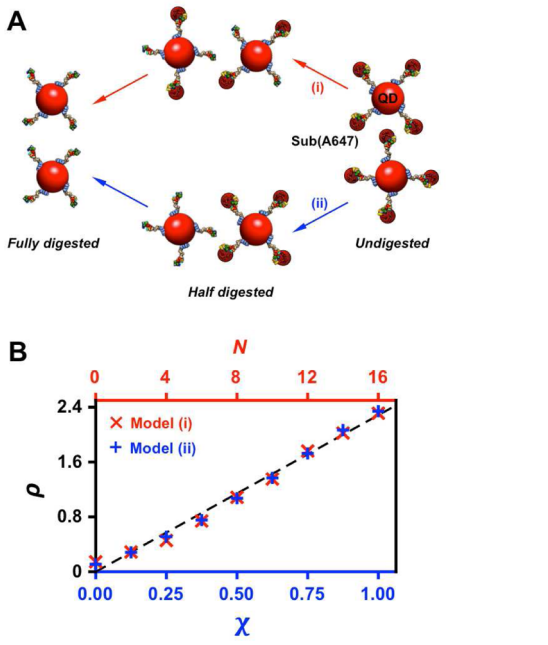

Figure 2. (A) Two possible models of proteolysis and corresponding methods of calibration. (i) Digestion of Sub(A647) conjugated to X–QD624 through multiple encounters between each X–QD624 and protease, with hydrolysis of only a single Sub(A647) in each interaction. (ii) Digestion of Sub(A647) conjugated to X–QD624 through a series of interactions where the protease hydrolyzes all of the Sub(A647) conjugated to a X–QD624 in a single interaction. This model is referred to as hopping. (B) Representative calibration data for GSH–QD624–$[Sub(A647)]_{16}$ with thrombin. For model (i), FRET ratios, ρ, were calibrated by mixing N and $N_0 - N$ equivalents of Sub(A647) and predigested peptide fragments, respectively, with X–QD624. For model (ii), FRET ratios were calibrated by mixing χ and $1 - \chi$ equivalents of X–QD624–$[Sub(A647)]_{16}$ conjugates and predigested conjugates, respectively. The same concentration of X–QD624 was used for both calibrations.

this reason, the progress curves for proteolytic activity that we present below have two y-axis scales: a left-hand scale that corresponds to N, the average number of Sub(A647) per QD624, for the model illustrated in Figure 2A(i), and a right-hand scale that corresponds to the concentration of X–QD624–$[Sub(A647)]_{16}$ remaining, assuming the model illustrated in Figure 2B(ii). The latter was a function of the χ value determined from the A647/QD624 PL ratio.

Proteolytic Assays. Progress curves for the digestion of X–QD624–$[Sub(A647)]_{16}$ conjugates as a function of thrombin and trypsin concentration are shown in Figure 3A,B. These curves were calculated from FRET data in terms of N, the average number of peptide substrates remaining per X–QD624 according to model (i) in Figure 2A, and [*], the remaining concentration of X–QD624–$[Sub(A647)]_{16}$ according to model (ii) in Figure 2A. As expected, more substrate was digested with increasing time, and, for each ligand coating, the rate of digestion scaled in proportion to the concentration of protease added. However, significant differences in proteolytic rate were observed between different ligand coatings for equal amounts of protease.

As per a conventional analysis of simple single-substrate enzyme kinetics within the framework of the Michaelis–Menten (MM) model, initial rates of hydrolysis of Sub(A647) by trypsin and thrombin were calculated from progress curves and are plotted in Figure 3C,D (note that the left axes, dN/dt, were converted to $d[S]/dt = [QD]\ dN/dt$ to obtain units of concentration). These plots permitted estimation of apparent specificity constants, k_{cat}/K_m, for the proteases with the X–QD624–$[Sub(A647)]_{16}$ conjugates, according to eq 4, where v is the initial rate of hydrolysis, [S] and [E] are the initial concentrations of substrate and enzyme, respectively, K_m is the Michaelis constant, k_{cat} is the turnover number, and $[S] \ll K_m$. Calculated specificity constants are listed in Table 1. The values are independent of the models in Figure 2A; however, given the nature of the system, these values should be interpreted as apparent pseudo-second-order rate constants rather than classical specificity constants (see Discussion for details). Both proteases had the same general trend in proteolytic activity as a function of ligand coating, with activity increasing in the order MPA < DHLA < CYS < GSH.

$$v = \frac{k_{cat}[E][S]}{K_m + [S]} \approx \frac{k_{cat}}{K_m}[E][S] \quad (4)$$

Despite the similar trend in relative activity between ligand coatings for trypsin and thrombin, the progress curves revealed important differences between the two proteases. First, trypsin was more robust than thrombin, exhibiting significant activity across all four ligand coatings, whereas several concentrations of thrombin that exhibited significant activity with the GSH and CYS coatings were completely inactive with the DHLA and MPA coatings. Furthermore, for each ligand, the progress curves for trypsin exhibited a much greater degree of convergence at complete turnover of available substrate (i.e., progress curves approach zero at long incubation times). In contrast, the progress curves for thrombin proteolysis often failed to converge or reach complete turnover, with the exception of the highest concentrations of thrombin with X = GSH, CYS, and DHLA. These results suggested that trypsin and thrombin had significantly different interactions with the X–QD624–Sub(A647) conjugates.

Adsorption of Thrombin and Trypsin on QDs. To account for the differences between thrombin and trypsin in Figure 3, we hypothesized that thrombin had stronger nonspecific interactions with the X–QD624, in addition to its selective enzyme–substrate interaction with the conjugated Sub(A647). This hypothesis was evaluated with electrophoretic mobility shift assays. Adsorption of protease on X–QD624 was expected to result in decreased mobility versus a X–QD624-only reference sample because of the increase in size upon protein adsorption.[27] QDs coated with all four ligands exhibited negative electrophoretic mobility in running buffer at pH 8.5, consistent with their anionic character. Initial tests were done with X–QD624 mixed with 100 μM thrombin and 1.2 μM trypsin (concentrations 5-fold larger than the highest concentrations used in Figure 3). For thrombin with each X–QD624, the gels showed mobility shifts indicative of adsorption on the QD (see Supporting Information, Figure S3). It was also noted that GSH–QD624 were least prone to adsorption and that MPA–QD624 were the most prone to adsorption, suggesting an inverse correlation between proteolytic rates and the strength of adsorption. For trypsin, no mobility shifts were observed.

Given the above results, electrophoretic mobility shifts were measured as a function of thrombin and trypsin concentration. Figure 4 shows the results when GSH– and MPA–QD624 were preincubated with either trypsin or thrombin at

DOI: 10.1021/am507466b
ACS Appl. Mater. Interfaces 2015, 7, 2535–2545

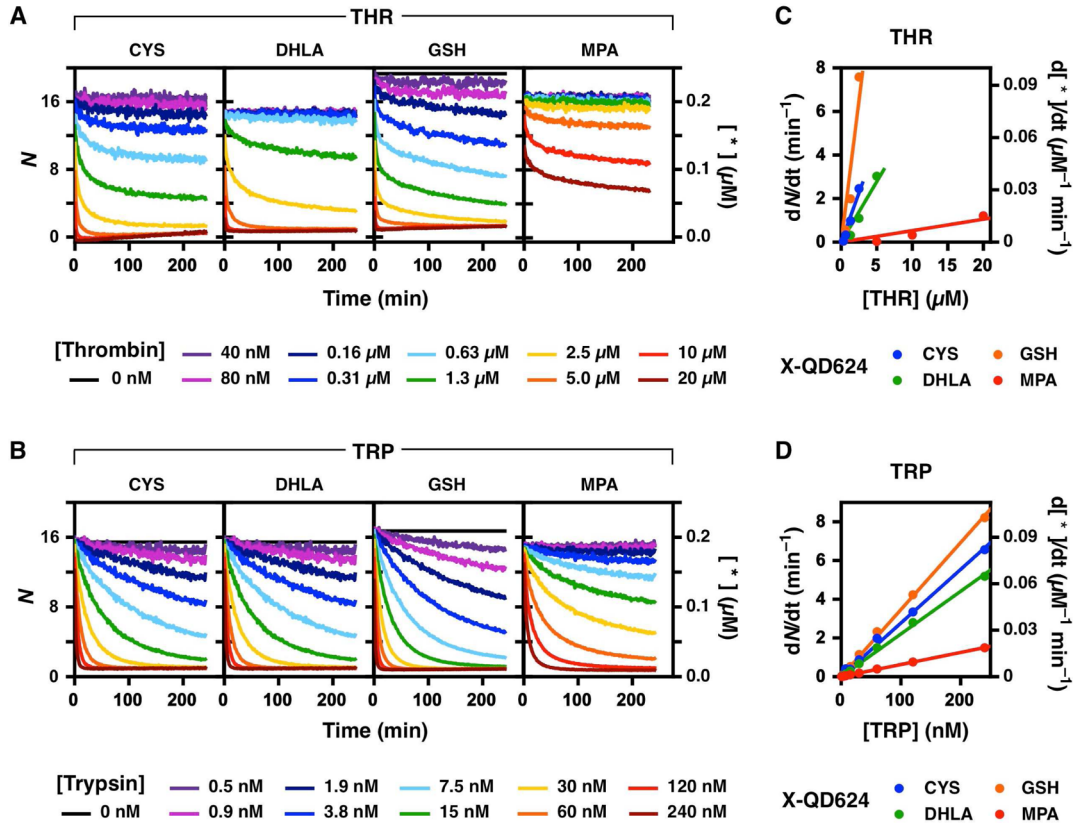

Figure 3. (A) Representative progress curves for the digestion of X−QD−-[Sub(A647)]$_{16}$ by different concentrations of thrombin. N is the number of Sub(A647) per QD, and [*] is the approximate concentration of X−QD−[Sub(A647)]$_{16}$. (B) Representative progress curves for the digestion of X−QD−[Sub(A647)]$_{16}$ by different concentrations of trypsin. (C) Plots of initial rates as a function of thrombin concentration, determined from the progress curves in panel A. (D) Plots of initial rates as a function of trypsin concentration, determined from the progress curves in panel B.

Table 1. Apparent Specificity Constants, k_{cat}/K_m, for X−QD624−Sub(A647)$_{16}$ Conjugates and Apparent Dissociation Constants, K_d, for X−QD524, Estimated from Initial Rates of Proteolytic Digestion with Thrombin and Trypsin

	thrombin		trypsin	
	k_{cat}/K_m (min^{-1} μM^{-1})[a]	K_d (μM)[b]	k_{cat}/K_m (min^{-1} μM^{-1})[a]	K_d (μM)[b]
CYS−QD	0.057 ± 0.005	0.20 ± 0.03	1.7 ± 0.1	
DHLA−QD	0.035 ± 0.004	0.03 ± 0.01	1.4 ± 0.1	0.8 ± 0.1
GSH−QD	0.16 ± 0.03	0.53 ± 0.01	2.2 ± 0.1	5.0 ± 1.6
MPA−QD	0.003 ± 0.001	0.09 ± 0.01	0.39 ± 0.01	1.1 ± 0.3

[a]Derived from the data in Figure 3 for X−QD624. [b]Derived from the data in Figure 5 for X−QD524. The listed uncertainties are standard errors from data fitting.

concentrations in the range 0.1−33 μM. Similar gels for CYS− and DHLA−QD624 with thrombin can be found in the Supporting Information (Figure S4). Mobility shifts from thrombin adsorption on X−QDs became evident at enzyme concentrations of ∼0.1 μM for MPA, ∼0.75 μM for DHLA and CYS, and ∼2.0 μM for GSH (Figure 4A). This trend was in agreement with the thrombin digestion rates in Figure 3, where MPA−QD624 yielded the slowest rates, DHLA−QD624 and CYS−QD624 yielded intermediate rates, and GSH−QD624 yielded the fastest rates. In the case of trypsin, the onset of adsorption on MPA−QD624 and GSH−QD624 occurred at higher concentrations than that for thrombin, with changes in the mobility becoming evident at ∼1 and ∼6 μM, respectively (Figure 4B), where the adsorption of trypsin appeared to result in aggregates of QD624 rather than a discrete shift of the band on the gel. Importantly, the result that trypsin adsorbed more readily on MPA−QD624 than GSH−QD624 was in agreement with the slower rates of digestion with the former, consistent with the results obtained with thrombin. The overall lower tendency of trypsin to adsorb to X−QD624 was also consistent with the smaller effect that QD ligand selection had on the rates of trypsin digestion.

In light of the apparent adsorption of thrombin on X−QD624, an important consideration was whether the adsorbed thrombin retained its structure. Attempts to characterize the adsorption of thrombin and trypsin on QDs using circular dichroism spectroscopy were unsuccessful because of the overwhelming background UV absorption of the QDs. Measurements of tryptophan fluorescence, which can sometimes serve as a probe of protein structure,[28] were also inconclusive.

Inhibition Assays. To better characterize the effect of QD ligand coatings and interfacial adsorption on protease activity, green-emitting X−QD524 were prepared without conjugated

DOI: 10.1021/am507466b
ACS Appl. Mater. Interfaces 2015, 7, 2535−2545

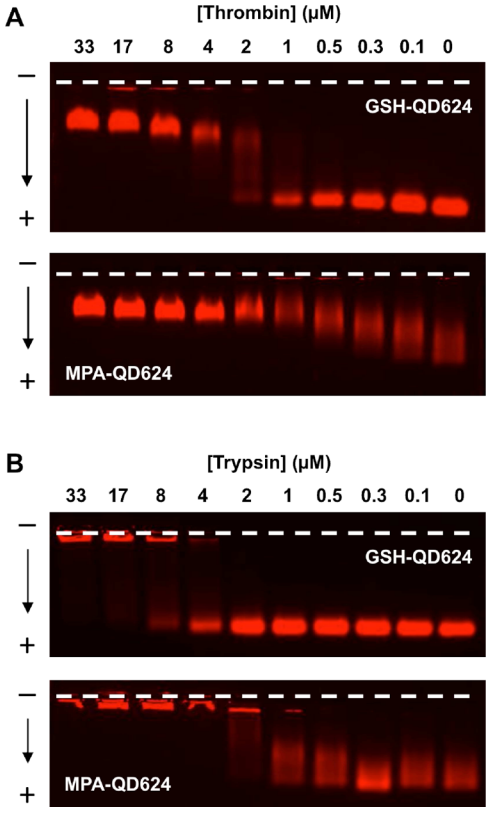

Figure 4. Pseudocolor PL images of agarose gels (1.0% w/v) showing changes in the electrophoretic mobility of GSH−QD624 and MPA−QD624 (0.2 μM) with different concentrations of (A) thrombin and (B) trypsin. Gels for thrombin with CYS−QD624 and DHLA−QD624 can be found in the Supporting Information. The dashed line indicates the position of the sample wells; the arrow at the left indicates the polarity of the electric field (7.3 V cm^{-1}). The gels clearly show that thrombin has a greater tendency to adsorb than trypsin and that adsorption is more favored on MPA−QD624 than GSH−QD624.

peptide and added to samples for FRET-based proteolytic assays with GSH−QD624−$[Sub(A647)]_{16}$. As illustrated in Figure 5A, our hypothesis was that if ligands on the QD promoted the adsorption of thrombin or trypsin, then these nonsubstrate X−QD524 would act as competitive inhibitors. The potency of the inhibition would depend on the selection of ligand and the tendency of the protease to adsorb. The spectrally narrow PL of the QD524 avoided interference with transduction of proteolysis via the QD624−A647 FRET pair, and, by virtue of using QDs with an alloyed CdSeS core, the QD524 and QD624 had approximately the same size (~6 nm) and surface areas for adsorption,[29] despite their spectrally distinct emission bands. GSH−QD624 were selected as the substrate-bearing QD because both thrombin and trypsin had the greatest activity with this ligand (see Figure 3).

To carry out the inhibition assays described above, the GSH−QD624−$[Sub(A647)]_{16}$ conjugates and protease were held at a fixed concentration, and increasing concentrations of X−QD524 were added as inhibitors. Figure 5B shows that, for thrombin, the rate of proteolytic digestion of GSH−QD624−$[Sub(A647)]_{16}$ decreased as the concentration of each inhibitor X−QD524 increased. Presumably, the formation of adsorption complexes between X−QD524 and thrombin increased as the concentration of X−QD524 increased, resulting in a reduction in the activity of thrombin. Qualitatively, the observed degree of inhibition in Figure 5B correlated with the observed rate of proteolysis in Figure 3A, with X = GSH and CYS having the smallest inhibitory effects, and X = DHLA and MPA having the largest effects. Figure 5C shows the results of analogous inhibition experiments with trypsin. As expected from the results in Figure 3B, the various X−QD524 had a much smaller inhibitory effect on trypsin activity. Even the highest concentrations of GSH− and CYS−QD524 had little effect on the trypsin activity toward GSH−QD624−$[Sub(A647)]_{16}$ conjugates. Although X = DHLA and MPA had some inhibitory effect, it was much less than with thrombin.

To quantitatively analyze thrombin and trypsin inhibition by the various QD coatings, we started from eq 5, which was reported by Gray et al. for the analysis of acetylcholinesterase inhibition.[30] In this model, [I] is the concentration of X−QD524, and K_d is the dissociation constant of the inhibitory interaction between thrombin and X−QD524. For $[S] \ll K_m$, eq 5 reduced to eq 6. Initial rates calculated for the progress curves in Figure 5B,C are shown in Figure 5D,E. These data were fit to eq 6, and the resulting values of K_d are listed in Table 1. Apparent K_d values for thrombin were on the order of 10^1 to 10^2 nM, whereas those for trypsin were ≥1 μM. The magnitudes of these values were consistent with expectations from electrophoretic mobility data. Although the trend in K_d did not exactly correlate with the trends from the proteolytic assays or mobility shift assays, there was once again a clear dichotomy between X = GSH and CYS and X = DHLA and MPA.

$$v = \frac{k_{cat}[E][S]}{K_m(1 + [S]K_m^{-1} + [I]K_d^{-1})} \quad (5)$$

$$v = \frac{(k_{cat}/K_m)[E][S]}{1 + [I]K_d^{-1}} \quad (6)$$

Comparing QD−Sub(A647) and Sub(A647). The results presented thus far have demonstrated that the adsorption of proteases on QDs can strongly affect the kinetics of proteolysis. In particular, ligand coatings that promoted adsorption inhibited proteolysis relative to coatings that had weaker adsorption; however, these results have thus far been presented without a baseline for comparison. To this end, we compared the rate of proteolysis associated with GSH−QD624−$[Sub(A647)]_{16}$ conjugates with an equivalent amount of Sub(A647) (without QDs) in bulk solution. To analyze proteolytic rates in bulk solution, substrate peptides were first hydrolyzed by the addition of thrombin or trypsin for a certain time interval (2, 5, 8, 15, 20, 40, 60, and 80 min) followed by termination of the reaction with the addition of TLCK, an irreversible protease inhibitor. GSH−QD624 were then added, and any non-hydrolyzed substrate assembled to the QDs to form GSH−QD624−$[Sub(A647)]_N$ FRET pairs and provide a readout signal analogous to the kinetic experiments with X−QD624 present throughout. Each of these assays was done in triplicate. Compared to the rate of digestion of GSH−QD624−$[Sub(A647)]_{16}$ conjugates, a much slower rate of proteolysis was observed when thrombin and trypsin were mixed with Sub(A647) in bulk solution without QDs, as shown in Figure 6. The results of these experiments were confirmed using a second measurement method that did not involve QDs at any step (see Supporting Information for details). These results are also shown in Figure 6 and were in good agreement with the results of the first analysis. The specificity constants, k_{cat}/K_m, for

DOI: 10.1021/am507466b
ACS Appl. Mater. Interfaces 2015, 7, 2535−2545

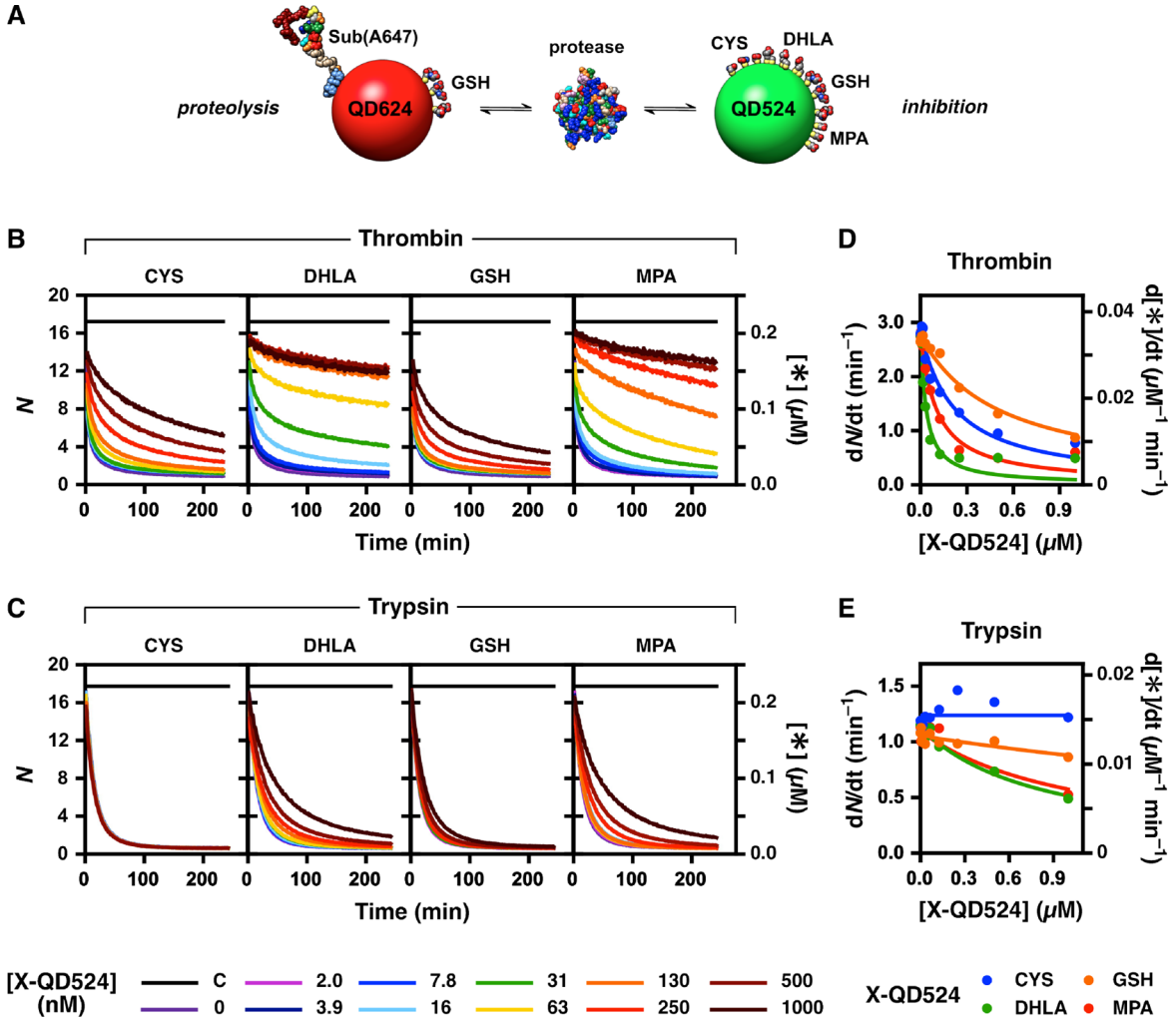

Figure 5. (A) Schematic of the QD inhibition experiment. Thrombin (THR) or trypsin (TRP) can adsorb on GSH−QD624−$[Sub(A647)]_{16}$ where it can hydrolyze substrate, or it can adsorb on X−QD524 where it cannot hydrolyze substrate. (B) Representative progress curves for the digestion of GSH−QD624−$[Sub(A647)]_{16}$ by thrombin in the presence of different concentrations of X−QD524. *N* is the number of Sub(A647) per QD624, and [*] is the approximate concentration of X−QD624−$[Sub(A647)]_{16}$. (C) Representative progress curves for the digestion of GSH−QD624−$[Sub(A647)]_{16}$ by trypsin in the presence of different concentrations of X−QD524. (D) Plots of initial rates as a function of X−QD524 concentration, determined from mathematical fitting of the progress curves in panel B (see Experimental Section). (E) Plots of initial rates as a function of X−QD524 concentration, determined from mathematical fitting of the progress curves in panel C.

Sub(A647) were calculated from Michaelis−Menten model fits to the progress curves, yielding values of ca. 0.002 min^{-1} μM^{-1} with thrombin and ca. 0.033 min^{-1} μM^{-1} with trypsin. The corresponding values for thrombin with MPA−QD624−$[Sub(A647)]_{16}$ and GSH−QD624−$[Sub(A647)]_{16}$ were 1.5- and 80-fold larger, respectively, and those values for trypsin were 12- and 65-fold larger (see Table 1). X−QD624 can thus provide either a drastic or modest acceleration of proteolytic activity depending on the selection of X and the protease.

DISCUSSION

Our results have shown that adsorption of a protease on a QD probe can have a profound effect on its proteolytic activity. It appears that, up to a point, affinity between the protease and the QD−peptide substrate conjugate can significantly accelerate proteolysis when compared to that in bulk solution; however, too much affinity for the QD interface may start to inhibit proteolysis. The accelerations seen in our experiments are more than an order of magnitude larger than the 2- to 3-fold increases that have been observed previously.[17,18] Our experiments have also shown that the degree of acceleration can vary significantly between two different proteases, independent of their preference for the substrate peptide conjugated to the QD. In a bioanalytical context, these observations suggest that the surface chemistry on QDs and other nanoparticles can provide a means of tuning the sensitivity and selectivity of assays, such that the activity of a target protease can be detected in the presence of a nontarget protease that has similar substrate specificity. Here, we discuss possible reasons for the different sensitivities of thrombin and trypsin toward the ligand coating on the QD probe and possible reasons for the higher levels of activities observed with CYS and GSH coatings versus DHLA and MPA coatings. Ramifications for understanding the mechanism of proteolysis with nanoparticle−peptide substrate conjugates are discussed in closing.

Differences between Thrombin and Trypsin. Bovine trypsin is a 23 kDa protein with a pI of ca. 10.5, and bovine thrombin is a 37 kDa protein with a pI of ca. 7. Both thrombin and trypsin hydrolyze peptide bonds C-terminal to arginine or

DOI: 10.1021/am507466b
ACS Appl. Mater. Interfaces 2015, 7, 2535−2545

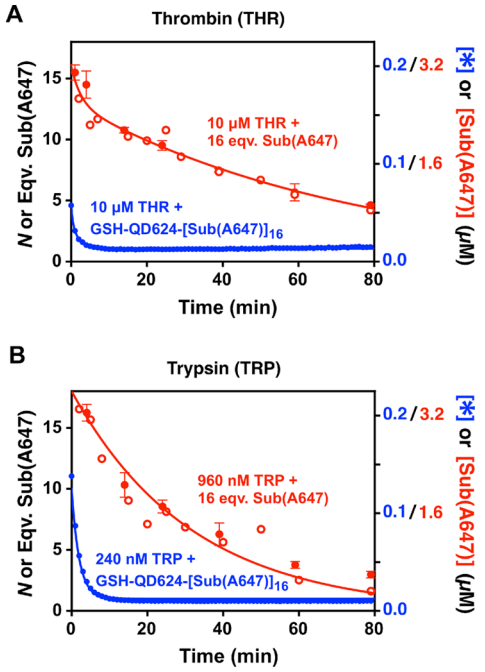

Figure 6. Progress curves for the activity of (A) thrombin (THR) and (B) trypsin (TRP) with GSH−QD−Sub(A647) conjugates (blue circles) and with an equivalent amount of Sub(A647) in bulk solution (red symbols). The activity in the latter case was determined by FRET measurements with QDs after the enzyme reaction had been quenched (closed red circles) and by using a pull-down assay with an affinity resin and absorption spectrophotometry (open red circles). Protease concentrations are indicated in the figure. The progress curves for the GSH−QD−Sub(A647) conjugates are from Figure 3. [*] is defined as per Figure 3.

lysine residues.[31,32] Thrombin has a preference for the cleavage site P4-P3-Pro-Arg-P1′-P2′, with hydrophobic residues at P4 and P3 and nonacidic residues at P1′ and P2′.[32] Although trypsin exhibits different hydrolytic rates with different substrates, its specificity for P4-P3-P2-Arg/Lys-P1′-P2′ is very broad, albeit with poor tolerance for Pro at the P1′ position and unfavorable interactions with acidic residues on either side of the cleavage site.[33] The LVPRGS sequence used in this study was thus a good substrate for both thrombin and trypsin.

One obvious difference between thrombin and trypsin in this study is that the latter hydrolyzes Sub(A647) more rapidly. This difference in activity toward Sub(A647) in bulk solution is trivial and can be attributed to the intrinsically different catalytic activities of thrombin and trypsin and the different degrees to which bulk assay conditions (e.g., pH) are optimal for these proteases. The more interesting difference is that thrombin adsorbs more strongly on X−QD624 and is more sensitive to changes in the identity of the ligand coating, X. At pH 8.5, trypsin will have a net positive charge, and an electrostatic attraction to the anionic X−QD624 may be sufficient to explain the relatively weak adsorption that was observed. Although thrombin has a net negative charge at pH 8.5, electrostatic repulsion does not appear to hinder its adsorption. This observation is not surprising given that thrombin has two positively charged anion binding exosites that interact with ligands such as polyphosphate,[34] hirudin,[35] heparin and heparan sulfate,[36,37] many other anionic macromolecules, and anionic surfaces such as glass.[38] In contrast to thrombin, trypsin does not have anion binding exosites.[39,40] Electrostatic potential maps[41] for thrombin and trypsin are shown in Figure 7 (generated from Protein Data Bank entries[42,43]), illustrating

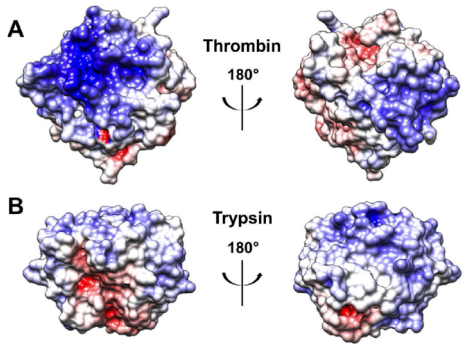

Figure 7. Surface electrostatic potential maps for (A) thrombin (Protein Data Bank ID: 1HRT) and (B) trypsin (Protein Data Bank ID: 1S0R). Positive, neutral, and negative potentials are colored blue, white, and red, respectively. Note the two strongly positive sites on thrombin, which are anion-binding exosites.

this difference. The observed adsorption of thrombin on the interface of QDs coated with anionic ligands is therefore consistent with its structure and function. We posit that the anion binding exosites of thrombin are the cause of its strong adsorption on anionic X−QD624 and, at least in part, are the reason for the greater dependence of its activity on the identity of X. More generally, similar differences in sensitivity to the coating on a nanoparticle might be expected between other enzymes of the same classes as trypsin and thrombin. The fibrinolytic and blood coagulation proteases (e.g., thrombin) have large, noncatalytic segments appended to a trypsin-homologue region, and these segments mediate binding to macromolecules and interfaces as part of the regulatory role of these proteases.[44] Digestive enzymes (e.g., trypsin) lack these segments in their structure.[44]

Differences between X−QDs. CYS, DHLA, GSH, and MPA ligands bind to the ZnS shell of QDs through their thiol groups and expose anionic carboxylate groups to bulk solution. CYS and GSH may also expose cationic amine groups. The X−QDs are stabilized as a uniform dispersion by net electrostatic repulsion between particles. CYS has pK_a values of 2.0 (−COOH) and 10.3 ($-NH_3^+$),[45] GSH has pK_a values of 2.1, 3.6 (−COOH), and 8.8 ($-NH_3^+$),[46] and DHLA and MPA have pK_a values of 4.8[47] and 4.7,[48] respectively. A simple Henderson−Hasselbalch calculation with these values suggests that each X−QD624 will carry 0.2, 1, 1.3, and 1 negative charge per CYS, DHLA, GSH, and MPA ligand, respectively. An important caveat to this analysis is that hydrogen bonding between ligands can elevate the pK_a values of carboxylic acid ligands on nanoparticles by several units relative to the values measured in bulk solution.[49] Indeed, it has been reported that MPA ligands on QDs exhibit behavior consistent with pK_a ∼ 8,[50] or 0.8 charges per ligand per QD at pH 8.5. The pK_a of amine groups may also be affected by hydrogen bonding between ligands and possible coordination to Zn sites on the QD surface. Experimentally, the relative electrophoretic mobilities of the X−QD624 were DHLA > GSH (0.9) > CYS (0.7) > MPA (0.6), where the values in parentheses indicate the migration distance relative to DHLA (see Supporting Information, Figure S3). Since all X−QD624 had the same hard geometric size, the differences in electrophoretic mobility were therefore a reflection of differences in charge and

DOI: 10.1021/am507466b
ACS Appl. Mater. Interfaces 2015, 7, 2535−2545

effective size in aqueous solution. A Ferguson analysis (see Supporting Information, Figure S6 and Table S3) indicated effective radii between 3.1 nm (GSH) and 4.9 nm (CYS) and zeta potentials ranging from −31 mV (MPA) to −37 mV (DHLA), in agreement with the trend in electrophoretic mobility. None of the above trends mirrored the trends observed for proteolytic activity: DHLA and GSH had the most comparable zeta potential but engendered very different proteolytic rates, whereas CYS and GSH had the most disparate effective radii but engendered the most similar proteolytic rates.

Potential gaps in ligand coverage also appear unlikely to be the cause of the observed trends in proteolytic rates. Both MPA and CYS are known to have tendencies to desorb from the QD surface, but they also engender very different proteolytic rates. Further evidence against gaps in ligand coverage mediating activity is that DHLA, which is bidentate and likely to be the most stable coating, has inhibitory effects comparable to those of MPA. It should also be noted that unbound ligands themselves cannot account for the observed effects on proteolysis. Control assays were done to measure the activity of thrombin toward *N*-benzoyl-Phe-Val-Arg-4-methoxy-β-naphthylamide hydrochloride, a fluorogenic small molecule substrate, in the presence of 2.5−40 μM of free ligand, X. This amount corresponded to the equivalent of 12−200 free ligands per X−QD624 in assays. As described in the Supporting Information (Figure S5), the effects of the free ligands on thrombin activity were inconsistent with the X−QD624 data.

Another possibility is that the substrate peptide, Sub(A647), adopted a different average conformation when assembled to the different X−QD624, with some conformations being more favorable for hydrolysis by trypsin and thrombin than others. Ligand-dependent orientation of a protein (~30 kDa) self-assembled to QDs with DHLA, GSH, and MPA ligands has been reported previously.[51] Here, the average center-to-center separation distances between X−QD624 and A647 with 16 Sub(A647) per QD were approximately 4.9, 7.6, 8.1, and 6.1 nm for X = CYS, DHLA, GSH, and MPA, respectively, as estimated from ensemble FRET efficiencies. The smallest and largest separations were for the CYS and GSH coatings, which yielded the highest levels of activity, suggesting that the trend in proteolytic activity was not due to differences in the average conformation of the peptide substrate.

Overall, the commonality appears to be that the two ligands that yield the highest levels of activity (CYS, GSH) have zwitterionic character, whereas the two ligands that yield the lowest levels of activity (DHLA, MPA) have purely anionic character. Zwitterionic surfaces, including those modified with CYS[52,53] and GSH,[54] have been reported to be resistant to nonspecific protein adsorption.[55,56] We suggest that the zwitterionic character of GSH and CYS ligands on X−QD624 tempers protease adsorption otherwise driven by the net charge on the QD, promoting increased proteolytic activity. Although detailed structures of nanoparticle interfaces are still poorly understood, our cumulative results are consistent with such a hypothesis.

On the Mechanism of Proteolysis. Our results are also consistent with, and provide further evidence to support, the hopping model that has been proposed for the proteolytic digestion of QD−peptide substrate conjugates.[18] This model, illustrated in Figure 2A(ii), stipulates that the conversion of each X−QD624−$[\text{Sub(A647)}]_{16}$ to X−QD624−$[\text{Sub(A647)}]_0$ occurs in the course of a single interaction between enzyme and QD. In contrast, the conventional model in Figure 2A(i) assumes that multiple interactions are required to achieve this net conversion, with each interaction converting X−QD624−$[\text{Sub(A647)}]_N$ to X−QD624−$[\text{Sub(A647)}]_{N-1}$. Attempts to use slab gel electrophoresis to resolve distinct populations of X−QD624−$[\text{Sub(A647)}]_{16}$ to X−QD624−$[\text{Sub(A647)}]_0$ during proteolysis were unsuccessful because of the limited resolution of the technique and the subtle changes in the size and charge of the QDs. Nonetheless, there are three strong indicators for a hopping model of proteolysis. First, the magnitude of the acceleration of proteolysis with QD−substrate peptide conjugates versus only substrate peptides in bulk solution. Diffusion-driven interactions between individual substrate peptides and protease cannot account for enhancements in activity of more than an order of magnitude when there are more than an order of magnitude fewer diffusing entities of X−QD624−$[\text{Sub(A647)}]_{16}$ than Sub(A647) alone (0.2 vs 3.2 μM in Figure 6). Second, the magnitude of the acceleration is sensitive to the surface chemistry of the QD. Since both Sub(A647) and the underlying QD624 were consistent between experiments, only the X ligand coating can be responsible for the observed trends in proteolytic activity. Third, thrombin and trypsin exhibit different sensitivities to the QD surface chemistry, indicating that the properties of the protease also play a role in determining the magnitude of acceleration. These results, including the direct observation of thrombin binding to X−QDs at assay-relevant concentrations, indicate an important role for interfacial chemistry in mediating observed rates of proteolysis. Such a dependence is consistent with a hopping model of proteolytic activity where the nanoparticle scaffold increases the colocalization of substrate and enzyme.

Given the above, our results also highlight the limitations of conventional Michaelis−Menten-type analyses that utilize initial rate data with QD−substrate conjugates and, likely, nanoparticle bioconjugates in general. Such analyses are semiquantitative because the complexities of the nanoparticle system are evident only by considering progress curves in full. The measured K_d values from initial rate data are approximate, much as the estimated or apparent values of specificity constants, k_{cat}/K_m, from initial rate data are better described as pseudo-second-order rate constants. Apparent values of k_{cat}/K_m are good for comparisons between systems but should not be interpreted as the same collection of physical constant(s) as k_{cat}/K_m for an enzyme−substrate reaction that meets the criteria of the Michaelis−Menten model. Our results indicate that a model that satisfactorily addresses nanoparticle systems of the type studied here must include provisions for adsorption and desorption of multiple protease molecules per nanoparticle and, if a hopping model is strictly correct, effectively undergo single-step conversion of QD−substrate conjugates to QD−product conjugates. There is also the possibility that the hopping model is mostly correct in that multiple substrates get digested per QD per encounter between QD and protease but is not always 100% per encounter as stipulated for pure hopping. The ideal experimental system for further studies would have high intrinsic activity, like the combination of trypsin and Sub(A647), such that progress curves could be measured in less than 1 to 2 h with less than one protease per QD, but have high-sensitivity to interfacial chemistry, like thrombin with X−QD624. Additional study is also needed to address the role of substrate density and its effect on apparent values of K_d and k_{cat}/K_m or if the surface

DOI: 10.1021/am507466b
ACS Appl. Mater. Interfaces 2015, 7, 2535−2545

chemistry on nanoparticles can be rationally controlled to target exosites on certain enzymes for specific enhancement or inhibition of only their activity. A full understanding of proteolysis associated with QD−peptide substrate conjugates may ultimately permit the design of bioanalytical probes with enhanced sensitivity and selectivity, potentially distinguishing between proteases with similar specificities when peptide probes alone cannot.

CONCLUSIONS

We studied the proteolytic activity of thrombin and trypsin toward X−QD624−$[Sub(A647)]_{16}$ conjugates, where X was CYS, DHLA, GSH, or MPA and Sub(A647) contained an LVPRGS amino acid sequence that was hydrolyzed by both proteases. QDs coated with GSH and CYS ligands exhibited the highest levels of proteolytic activity, whereas those with DHLA and MPA exhibited the lowest levels of proteolytic activity. Thrombin was more sensitive to changes in X, with a ca. 50-fold change in activity between coatings, versus only a 5-fold change for trypsin. Trends in thrombin and trypsin activity with changes in X, and the greater sensitivity of thrombin to X, were correlated with the apparent tendency of the protease to adsorb to the interface of the QD. This behavior was discussed in terms of the physicochemical characteristics of both the proteases and the ligand coatings. There was also a remarkable 65−80-fold increase in proteolytic activity for GSH−QD624−$[Sub(A647)]_{16}$ conjugates versus an equivalent amount of Sub(A647) in bulk solution. Analogous increases with MPA−QD624−$[Sub(A647)]_{16}$ were a more modest 1.5−12-fold better than that in bulk solution. Overall, these results show that nanoparticle surface chemistry plays an important role in mediating substrate turnover, providing some of the strongest support to date for a hopping-like model of hydrolytic enzyme activity with nanoparticle−substrate conjugates.

ASSOCIATED CONTENT

Supporting Information

Additional experimental methods, properties of the X−QD624−A647 FRET pairs, calibration curves, gel electrophoresis results, additional proteolytic assays, and Ferguson analysis. This material is available free of charge via the Internet at http://pubs.acs.org.

AUTHOR INFORMATION

Corresponding Author

*E-mail: algar@chem.ubc.ca.

Notes

The authors declare no competing financial interest.

ACKNOWLEDGMENTS

The authors acknowledge support for this research from the Natural Sciences and Engineering Research Council of Canada (NSERC), the Canada Foundation for Innovation (CFI), and the University of British Columbia. W.R.A. is grateful for a Canada Research Chair (Tier 2) and a Michael Smith Foundation for Health Research Scholar Award. Molecular graphics and analyses were performed with the UCSF Chimera package. Chimera is developed by the Resource for Biocomputing, Visualization, and Informatics at the University of California, San Francisco (supported by NIGMS P41-GM103311).

REFERENCES

(1) Petryayeva, E.; Algar, W. R.; Medintz, I. L. Quantum Dots in Bioanalysis: A Review of Applications across Various Platforms for Fluorescence Spectroscopy and Imaging. *Appl. Spectrosc.* **2013**, *67*, 215−252.

(2) Mattoussi, H.; Palui, G.; Na, H. B. Luminescent Quantum Dots as Platforms for Probing in Vitro and in Vivo Biological Processes. *Adv. Drug Delivery Rev.* **2012**, *64*, 138−166.

(3) Zrazhevskiy, P.; Sena, M.; Gao, X. H. Designing Multifunctional Quantum Dots for Bioimaging, Detection, and Drug Delivery. *Chem. Soc. Rev.* **2010**, *39*, 4326−4354.

(4) Kim, G. B.; Kim, Y. P. Analysis of Protease Activity Using Quantum Dots and Resonance Energy Transfer. *Theranostics* **2012**, *2*, 127−138.

(5) Lee, S.; Cha, E. J.; Park, K.; Lee, S. Y.; Hong, J. K.; Sun, I. C.; Kim, S. Y.; Choi, K.; Kwon, I. C.; Kim, K.; Ahn, C. H. A Near-Infrared-Fluorescence-Quenched Gold-Nanoparticle Imaging Probe for in Vivo Drug Screening and Protease Activity Determination. *Angew. Chem., Int. Ed.* **2008**, *47*, 2804−2807.

(6) Wang, H. B.; Zhang, Q.; Chu, X.; Chen, T. T.; Ge, J.; Yu, R. Q. Graphene Oxide−Peptide Conjugate as an Intracellular Protease Sensor for Caspase-3 Activation Imaging in Live Cells. *Angew. Chem., Int. Ed.* **2011**, *50*, 7065−7069.

(7) Algar, W. R.; Kim, H.; Medintz, I. L.; Hildebrandt, N. Emerging Non-traditional Förster Resonance Energy Transfer Configurations with Semiconductor Quantum Dots: Investigations and Applications. *Coord. Chem. Rev.* **2014**, *263−264*, 65−85.

(8) Medintz, I. L.; Clapp, A. R.; Brunel, F. M.; Tiefenbrunn, T.; Uyeda, H. T.; Chang, E. L.; Deschamps, J. R.; Dawson, P. E.; Mattoussi, H. Proteolytic Activity Monitored by Fluorescence Resonance Energy Transfer through Quantum-Dot−Peptide Conjugates. *Nat. Mater.* **2006**, *5*, 581−589.

(9) Shi, L. F.; De Paoli, V.; Rosenzweig, N.; Rosenzweig, Z. Synthesis and Application of Quantum Dots FRET-Based Protease Sensors. *J. Am. Chem. Soc.* **2006**, *128*, 10378−10379.

(10) Chang, E.; Miller, J. S.; Sun, J.; Yu, W. W.; Colvin, V. L.; Drezek, R.; West, J. L. Protease-Activated Quantum Dot Probes. *Biochem. Biophys. Res. Commun.* **2005**, *334*, 1317−1321.

(11) Gill, R.; Willner, I.; Shweky, I.; Banin, U. Fluorescence Resonance Energy Transfer in CdSe/ZnS-DNA Conjugates: Probing Hybridization and DNA Cleavage. *J. Phys. Chem. B* **2005**, *109*, 23715−23719.

(12) Huang, S.; Xiao, Q.; He, Z. K.; Liu, Y.; Tinnefeld, P.; Su, X. R. A High Sensitive and Specific QDs FRET Bioprobe for MNase. *Chem. Commun.* **2008**, 5990−5992.

(13) Lowe, S. B.; Dick, J. A. G.; Cohen, B. E.; Stevens, M. M. Multiplex Sensing of Protease and Kinase Enzyme Activity via Orthogonal Coupling of Quantum Dot Peptide Conjugates. *ACS Nano* **2012**, *6*, 851−857.

(14) Kim, Y. P.; Oh, Y. H.; Oh, E.; Ko, S.; Han, M. K.; Kim, H. S. Energy Transfer-Based Multiplexed Assay of Proteases by Using Gold Nanoparticle and Quantum Dot Conjugates on a Surface. *Anal. Chem.* **2008**, *80*, 4634−4641.

(15) Boeneman, K.; Mei, B. C.; Dennis, A. M.; Bao, G.; Deschamps, J. R.; Mattoussi, H.; Medintz, I. L. Sensing Caspase 3 Activity with Quantum Dot−Fluorescent Protein Assemblies. *J. Am. Chem. Soc.* **2009**, *131*, 3828−3829.

(16) Johnson, B. J.; Algar, W. R.; Malanoski, A. P.; Ancona, M. G.; Medintz, I. L. Understanding Enzymatic Acceleration at Nanoparticle Interfaces: Approaches and Challenges. *Nano Today* **2014**, *9*, 102−131.

(17) Prigodich, A. E.; Alhasan, A. H.; Mirkin, C. A. Selective Enhancement of Nucleases by Polyvalent DNA-Functionalized Gold Nanoparticles. *J. Am. Chem. Soc.* **2011**, *133*, 2120−2123.

(18) Algar, W. R.; Malanoski, A.; Deschamps, J. R.; Blanco-Canosa, J. B.; Susumu, K.; Stewart, M. H.; Johnson, B. J.; Dawson, P. E.; Medintz, I. L. Proteolytic Activity at Quantum Dot Conjugates: Kinetic Analysis Reveals Enhanced Enzyme Activity and Localized Interfacial "Hopping.". *Nano Lett.* **2012**, *12*, 3793−3802.

DOI: 10.1021/am507466b
ACS Appl. Mater. Interfaces 2015, 7, 2535−2545

(19) Chapman, H. A.; Riese, R. J.; Shi, G. P. Emerging Roles for Cysteine Proteases in Human Biology. *Annu. Rev. Physiol.* **1997**, *59*, 63−88.
(20) Hedstrom, L. Serine Protease Mechanism and Specificity. *Chem. Rev.* **2002**, *102*, 4501−4523.
(21) Nelson, A. R.; Fingleton, B.; Rothenbergy, M. L.; Matrisian, L. M. Matrix Metalloproteinases: Biologic Activity and Clinical Implications. *J. Clin. Oncol.* **2000**, *18*, 1135−1149.
(22) Earnshaw, W. C.; Martins, L. M.; Kaufmann, S. H. Mammalian Caspases: Structure, Activation, Substrates, and Functions During Apoptosis. *Annu. Rev. Biochem.* **1999**, *68*, 383−424.
(23) Overall, C. M.; Kleifeld, O. Validating Matrix Metalloproteinases as Drug Targets and Anti-targets for Cancer Therapy. *Nat. Rev. Cancer* **2006**, *6*, 227−239.
(24) Algar, W. R.; Blanco-Canosa, J. B.; Manthe, R. L.; Susumu, K.; Stewart, M. H.; Dawson, P. E.; Medintz, I. L. Synthesizing and Modifying Peptides for Chemoselective Ligation and Assembly into Quantum Dot−Peptide Bioconjugates. *Methods Mol. Biol.* **2013**, *1025*, 47−73.
(25) Jenny, R. J.; Mann, K. G.; Lundblad, R. L. A Critical Review of the Methods for Cleavage of Fusion Proteins with Thrombin and Factor Xa. *Protein Expression Purif.* **2003**, *31*, 1−11.
(26) Berlier, J. E.; Rothe, A.; Buller, G.; Bradford, J.; Gray, D. R.; Filanoski, B. J.; Telford, W. G.; Yue, S.; Liu, J. X.; Cheung, C. Y.; Chang, W.; Hirsch, J. D.; Beechem, J. M.; Haugland, R. P.; Haugland, R. P. Quantiative Comparison of Long-Wavelength Alexa Fluor Dyes to Cy Dyes: Fluorescence of the Dyes and Their Bioconjugates. *J. Histochem. Cytochem.* **2003**, *51*, 1699−1712.
(27) Prasuhn, D. E.; Deschamps, J. R.; Susumu, K.; Stewart, M. H.; Boeneman, K.; Blanco-Canosa, J. B.; Dawson, P. E.; Medintz, I. L. Polyvalent Display and Packing of Peptides and Proteins on Semiconductor Quantum Dots: Predicted versus Experimental Results. *Small* **2010**, *6*, 555−564.
(28) Vivian, J. T.; Callis, P. R. Mechanisms of Tryptophan Fluorescence Shifts in Proteins. *Biophys. J.* **2001**, *80*, 2093−2109.
(29) *Fluorescent Nanocrystal Specifications*; Cytodiagnostics, Inc.: Burlington, Ontario, Canada; http://www.cytodiagnostics.com/store/pc/Fluorescent-Nanocrystals-c17.htm (accessed 17 September 2014).
(30) Gray, P. J.; Duggleby, R. G. Analysis of Kinetic Data for Irreversible Enzyme Inhibition. *Biochem. J.* **1989**, *257*, 419−424.
(31) Olsen, J. V.; Ong, S. E.; Mann, M. Trypsin Cleaves Exclusively C-Terminal to Arginine and Lysine Residues. *Mol. Cell. Proteomics* **2004**, *3*, 608−614.
(32) Chang, J. Y. Thrombin Specificity Requirement for Apoloar Amino Acids Adjacent to the Thrombin Cleavage Site of Polypeptide Substrate. *Eur. J. Biochem.* **1985**, *151*, 217−224.
(33) Rodriguez, J.; Gupta, N.; Smith, R. D.; Pevzner, P. A. Does Trypsin Cut Before Proline? *J. Proteome Res.* **2008**, *7*, 300−305.
(34) Mutch, N. J.; Myles, T.; Leung, L. L. K.; Morrissey, J. H. Polyphosphate Binds with High Affinity to Exosite II of Thrombin. *J. Thromb. Haemostasis* **2010**, *8*, 548−555.
(35) Malovichko, M. V.; Sabo, T. M.; Maurer, M. C. Ligand Binding to Anion Binding Exosites Regulates Conformational Properties of Thrombin. *J. Biol. Chem.* **2013**, *288*, 8667−8678.
(36) Mosier, P. D.; Krishnasamy, C.; Kellogg, G. E.; Desai, U. R. On the Specificity of Heparin/Heparan Sulfate Binding to Proteins. Anion-Binding Sites on Antithrombin and Thrombin Are Fundamentally Different. *PLoS One* **2012**, *7*, e48632.
(37) Sheehan, J. P.; Sadler, J. E. Molecular Mapping of the Heparin-Binding Exosite of Thrombin. *Proc. Natl. Acad. Sci. U.S.A.* **1994**, *91*, 5518−5522.
(38) Waugh, D. F.; Anthony, L. J.; Ng, H. The Interactions of Thrombin with Borosilicate Glass Surfaces. *J. Biomed. Mater. Res.* **1975**, *9*, 511−536.
(39) Page, M. J.; DiCera, E. Is It Possible to Transform Trypsin to Thrombin? *IUBMB Life* **2007**, *59*, 413−414.
(40) Jenny, N. S.; Lundblad, R. L.; Mann, K. G. In *Hemostasis and Thrombosis: Basic Principles and Clinical Practice*, 5th ed.; Colman, R. W., Ed.; Lippincott Williams & Wilkins: Philadelphia, PA, 2006; Chapter 10, p 198.
(41) Pettersen, E. F.; Goddard, T. D.; Huang, C. C.; Couch, G. S.; Greenblatt, D. M.; Meng, E. C.; Ferrin, T. E. UCSF Chimera—A Visualization System for Exploratory Research and Analysis. *J. Comput. Chem.* **2004**, *25*, 1605−1612.
(42) Vitali, J.; Martin, P. D.; Malkowski, M. G.; Robertson, W. D.; Lazar, J. B.; Winant, R. C.; Johnson, P. H.; Edwards, B. F. The Structure of a Complex of Bovine alpha-Thrombin and Recombinant Hirudin at 2.8-Å Resolution. *J. Biol. Chem.* **1992**, *267*, 17670−17678.
(43) Chamorro, J. A.; Cueseta-Seijo, J. A.; Garca-Granda, S. Bovine Pancreatic Trypsin Inhibited with Benzamidine from Synchrotron Data. *Protein Data Bank* **2009**, DOI: 10.2210/pdb1s0r/pdb.
(44) Patthy, L. Evolution of the Proteases of Blood Coagulation and Fibrinolysis by Assembly from Modules. *Cell* **1985**, *41*, 657−663.
(45) Lide, D. R. *Handbook of Chemistry and Physics*, 72nd ed; CRC Press: Boca Raton, FL, 1991.
(46) Dawson, R. M. C. *Data for Biochemical Research*, 3rd ed; Oxford Univeristy Press: New York, 1987.
(47) Smith, A. R.; Shenvi, S. V.; Widlansky, M.; Suh, J. H.; Hagen, T. M. Lipoic Acid as a Potential Therapy for Chronic Diseases Associated with Oxidative Stress. *Curr. Med. Chem.* **2004**, *11*, 1135−1146.
(48) Burris, S. C.; Zhou, Y.; Maupin, W. A.; Ebelhar, A. J.; Daugherty, M. W. The Effect of Surface Preparation on Apparent Surface pK_a's of Omega-Mercatpocarboxylic Acid Self-Assembled Monolayers on Polycrystalline Gold. *J. Phys. Chem. C* **2008**, *112*, 6811−6815.
(49) Wang, D.; Nap, R. J.; Lagzi, I.; Kowalczyk, B.; Han, S.; Grzybowski, B. A.; Szleifer, I. How and Why Nanoparticle's Curvature Regulates the Apparent pK_a of the Coating Ligands. *J. Am. Chem. Soc.* **2011**, *133*, 2192−2197.
(50) Algar, W. R.; Krull, U. J. Characterization of the Adsorption of Oligonucleotides on Mercaptopropionic Acid-Coated CdSe/ZnS Quantum Dots Using Fluorescence Resonance Energy Transfer. *J. Colloid Interface Sci.* **2011**, *359*, 148−154.
(51) Zhang, Y.; Zhang, H.; Hollins, J.; Webb, M. E.; Zhou, D. Small-Molecule Ligands Strongly Affect the Förster Resonance Energy Transfer between a Quantum Dot and a Fluorescent Protein. *Phys. Chem. Chem. Phys.* **2011**, *13*, 19427−19436.
(52) Lin, P.; Ding, L.; Lin, C. W.; Gu, F. Nonfouling Property of Zwitterionic Cysteine Surface. *Langmuir* **2014**, *30*, 6497−6507.
(53) Murthy, A. K.; Stover, R. J.; Hardin, W. G.; Schramm, R.; Nie, G. D.; Gourisankar, S.; Truskett, T. M.; Sokolov, K. V.; Johnston, K. P. Charged Gold Nanoparticles with Essentially Zero Serum Protein Adsorption in Undiluted Fetal Bovine Serum. *J. Am. Chem. Soc.* **2013**, *135*, 7799−7802.
(54) Wang, J.; Dong, B. A.; Chen, B. T.; Xu, S.; Zhang, S.; Yu, W.; Xu, C. X.; Song, H. W. Glutathione Modified Gold Nanorods with Excellent Biocompatibility and Weak Protein Adsorption, Targeting Imaging and Therapy toward Tumor Cells. *Dalton Trans.* **2013**, *42*, 11548−11558.
(55) Garcia, K. P.; Zarschler, K.; Barbaro, L.; Barreto, J. A.; O'Malley, W.; Spiccia, L.; Stephan, H.; Graham, B. Zwitterionic-Coated "Stealth" Nanoparticles for Biomedical Applications: Recent Advances in Countering Biomolecular Corona Formation and Uptake by the Mononuclear Phagocyte System. *Small* **2014**, *10*, 2516−2529.
(56) Moyano, D. F.; Saha, K.; Prakesh, G.; Yan, B.; Kong, H.; Yazdani, M.; Rotello, V. M. Fabrication of Corona-Free Nanoparticles with Tunable Hydrophobicity. *ACS Nano* **2014**, *8*, 6748−6755.

DOI: 10.1021/am507466b
ACS Appl. Mater. Interfaces 2015, 7, 2535−2545